# Influence of reactor wall conditions on etch processes in inductively coupled fluorocarbon plasmas

M. Schaepkens, R. C. M. Bosch,[a] T. E. F. M. Standaert, and G. S. Oehrlein[b]
*Department of Physics, University at Albany, State University of New York, Albany, New York 12222*

J. M. Cook
*Lam Research Corporation, Fremont, California 94538-6470*

(Received 25 June 1997; accepted 30 January 1998)

The influence of reactor wall conditions on the characteristics of high density fluorocarbon plasma etch processes has been studied. Results obtained during the etching of oxide, nitride, and silicon in an inductively coupled plasma source fed with various feedgases, such as $CHF_3$, $C_3F_6$, and $C_3F_6/H_2$, indicate that the reactor wall temperature is an important parameter in the etch process. Adequate temperature control can increase oxide etch selectivity over nitride and silicon. The loss of fluorocarbon species from the plasma to the walls is reduced as the wall temperature increased. The fluorocarbon deposition on a cooled substrate surface increases concomitantly, resulting in a more efficient suppression of silicon and nitride etch rates, whereas oxide etch rates remain nearly constant. © *1998 American Vacuum Society.* [S0734-2101(98)03504-0]

## I. INTRODUCTION

Etching of trenches or contact holes into silicon dioxide is an indispensable process in modern integrated circuit fabrication technology. A high oxide etch rate and etch selectivity of oxide to silicon and nitride are important requirements that need to be met in order for etch processes to be applicable in industrial manufacturing. Etch processes employing low pressure high density fluorocarbon discharges are expected to meet these demands, and have been studied extensively.[1–6]

Low pressure high density fluorocarbon plasma processes, however, have been found to suffer from process drifts.[7] At low pressure, plasma-wall interactions are of significant importance in determining the discharge chemistry. Process drifts have been attributed to changes in reactor wall conditions.[8,9] In order to limit changes in reactor wall conditions and to create a stable and reproducible process environment, it is common in semiconductor processing to ''season'' a reactor. A fundamental understanding of the important mechanisms operating in the conditioning procedure is lacking, however.

This article presents results of a study of the influence of reactor wall conditions on the stability of etch processes. Results obtained during the etching of oxide, nitride, and silicon in an inductively coupled plasma source fed with various feedgases, such as $CHF_3$, $C_3F_6$, and $C_3F_6/H_2$, will be reported. Explanations of the observed effects will be presented.

## II. EXPERIMENTAL SETUP

The high-density plasma source used in this work is a radio frequency inductively coupled plasma (ICP) source of planar coil design. This plasma source has also been referred to in literature as transformer coupled plasma (TCP) and radio frequency induction (RFI) source. A schematic outline of the ICP reactor used is shown in Fig. 1. It is similar to the one described by Keller *et al.*[10]

The apparatus consists of an ultrahigh vacuum (UHV) compatible processing chamber in which the plasma source and a wafer holding electrostatic chuck are located. The center part of the ICP source is a planar, 160 mm diameter induction coil that is separated from the process chamber by a 19.6 mm thick, 230 mm diameter quartz window. The coil is powered through a matching network by a 13.56 MHz, 0–2000 W power supply. The results presented here were all obtained at an inductive power level of 1400 W.

A plasma confinement ring that can hold multipole magnets is located below the quartz window. For this work, no magnets were placed into the confinement ring, but the ring itself confines the plasma. The confinement ring has poor thermal contact with other parts of the reactor and its temperature cannot be controlled independently. In the rest of this article, the confinement ring will be referred to as the reactor wall (since this is the surface that the plasma is in contact with). The inner diameter of the confinement ring is 20 cm.

Wafers with diameters of 125 mm are placed on a bipolar electrostatic chuck during processing. The chuck is located 7 cm downstream from the ICP source and allows the wafer to be RF biased and cooled during processing. A helium pressure of 5 Torr is applied to the backside of the wafer during the experiment to achieve a good thermal conduction between the wafer and the chuck.[11] The electrostatic chuck is cooled by a refrigerator. A variable frequency RF power supply (500 kHz–40 MHz, 0–300 W) is used to bias the wafer for etching experiments. The experiments reported in this work were all performed at 3.4 MHz.

Substrates placed at the center of a wafer can be monitored by *in situ* ellipsometry. Plasma diagnostics like a retractable Langmuir probe and optical emission spectroscopy

[a]Permanent address: Eindhoven University of Technology, P.O. Box 513, 5600 MB Eindhoven, The Netherlands.
[b]Electronic mail: oehrlein@cnsibm.albany.edu

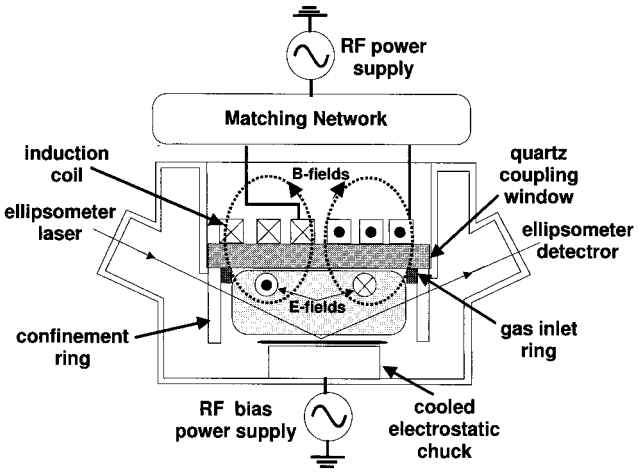


FIG. 1. Schematic of ICP source setup.

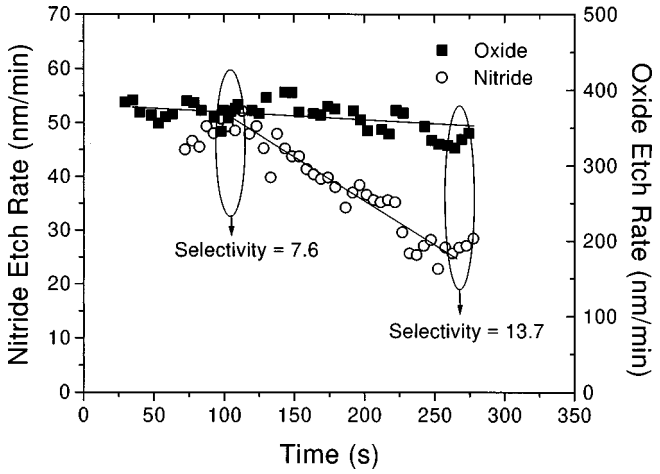


FIG. 2. Nitride etch rate and oxide etch rate as a function of the time that the plasma was switched on (1400 W inductive power, 6 mTorr operating pressure, −100 V self-bias).

(OES) can be used for gas-phase characterization. With the retractable Langmuir probe it is possible to make a scan of the ion current density over 70% of the wafer. The values reported here were measured in the center of the reactor, 2 cm above the wafer surface.

The process chamber is pumped using a 450 ℓ/s turbomolecular pump backed by a Roots blower and a mechanical pump. The process gases are admitted into the reactor through a gas inlet ring located just under the quartz window. The pressure is measured with a capacitance manometer. Pressure control is achieved by an automatic throttle valve in the pump line.

The ICP chamber is connected to a wafer handling cluster system that allows all sample transport to occur under ultrahigh vacuum conditions. Processed samples can be transported from the ICP reactor to a surface analysis chamber for X-ray photoelectron spectroscopy (XPS) without exposure to air.

## III. RESULTS AND DISCUSSION

### A. Investigation of process drift

It was found in an earlier study by this group that oxide could be etched at a high rate and at the same time selectively to nitride in a $C_3F_6/H_2$ (40 sccm/15 sccm) discharge at high inductive power (1400 W) and low operating pressure (6 mTorr) when a sufficiently high RF bias power (200 W corresponding to −100 V self-bias) is applied to the wafer.[12] In that study, however, the samples were etched for only a relatively small time period. When etching for longer times, it was observed that etch rates of both oxide and nitride were dependent on the time that the plasma was switched on; see Fig. 2. The nitride etch rate decreases significantly as a function of processing time, whereas the oxide etch rate remains at a near constant value. This results in an increase of oxide-to-nitride selectivity with etching time.

Two time-dependent processes were initially suggested to be responsible for the changes in etch characteristics as a function of time, namely (1) fluorocarbon contamination of the reactor walls during processing and (2) increasing temperature of the reactor. In order to distinguish between these processes, the following experiment was performed; see Fig. 3.

Blanket nitride samples were etched at the same conditions and the rates are plotted versus processing time. Results for three consecutive etch experiments are shown. The first experiment was performed starting with a reactor that has been cleaned with an oxygen plasma prior to the experiment. The reactor is initially at room temperature. In between experiments the reactor was allowed to cool down, but no oxygen plasma cleaning was performed.

It can be seen that during each run there is a significant decrease of the nitride etch rate. The initial value of the etch rate in each run stays at a constant level. This experiment

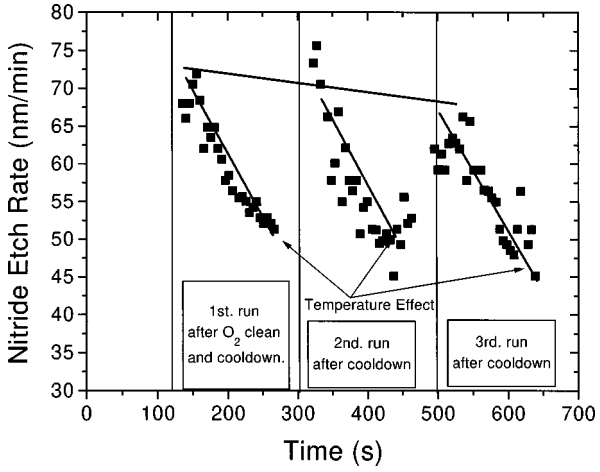


FIG. 3. Nitride etch rate as a function of processing time for three consecutive etch experiments. The first experiment was performed starting with a reactor that has no fluorocarbon material deposited at the walls (reactor was cleaned with an oxygen plasma). Between the etch experiments the reactor was allowed to cool to room temperature, but no oxygen plasma cleaning was performed (1400 W inductive power, 6 mTorr operating pressure, −100 V self-bias).

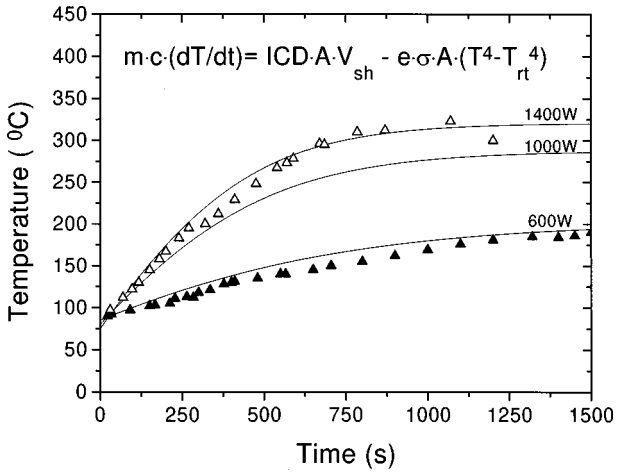


FIG. 4. Wall temperature as a function of processing time. The triangles are experimental data; the curves show the model.

shows that the heating of the reactor is the process that is dominant in producing the observed effect.

### B. Time dependence of the reactor wall temperature

The time dependence of the wall temperature has been measured by attaching a thermocouple to the confinement ring. The resulting data for both a 600 and 1400 W $C_3F_6/H_2$ (40 sccm/15 sccm) plasma at 6 mTorr operating pressure is plotted in Fig. 4. Similar experiments were obtained using different fluorocarbon gases, such as $CHF_3$ and $C_3F_6$. The time dependence of the reactor wall temperature changed little with feedgas chemistry.

A simple model that describes the time dependence of the wall temperature T has been developed. In the model it is assumed that the power dissipated in the wall results from collisions of ions with the wall. The ions have an energy equal to the sheath voltage between the floating wall and the plasma. The energy loss factor for the wall is assumed to be Stefan-Boltzmann radiation. The resulting differential equation is

$$m \cdot c \cdot dT/dt = \mathrm{ICD} \cdot A \cdot V_{\mathrm{sh}} - e \cdot \sigma \cdot A \cdot (T^4 - T_{\mathrm{RT}}^4), \qquad (1)$$

where $m$ is the mass of the confinement ring, $c$ is the heat capacitance of the anodized aluminum confinement ring, ICD is the ion current density, $A$ is the area of reactor wall, $V_{\mathrm{sh}}$ is the sheath voltage between the floating wall and the plasma, $e$ is the emissivity of the anodized aluminum confinement ring, $\sigma$ is the Stefan-Boltzmann constant, and $T_{\mathrm{RT}}$ is the room temperature.

The ion current density was measured by Langmuir probe measurement. The sheath voltage was calculated to be 15 V by using an estimated value of 3 eV for the electron temperature. Values between 0.4 and 0.5 for the emissivity were determined from the cooling rate of the wall after the plasma was shut off. The differential equation was solved numerically, resulting in the curves plotted in Fig. 4. The agreement between the model and the experimental data is satisfactory.

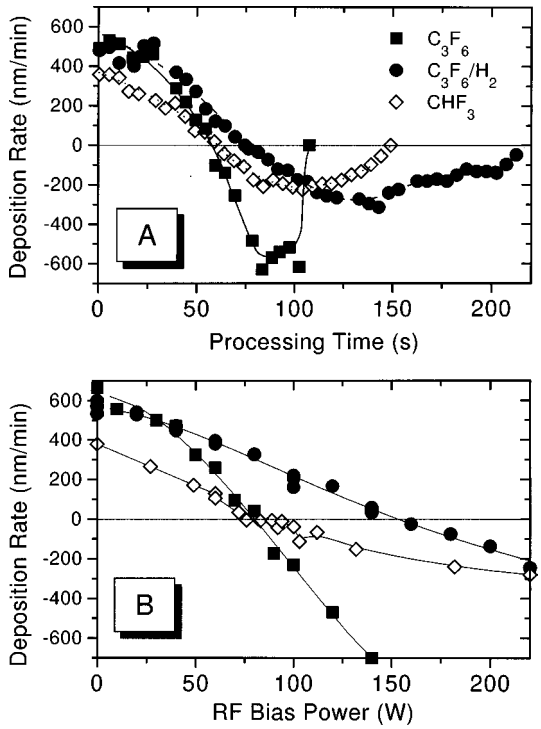


FIG. 5. (A) Passive deposition rates are measured as a function of time on a non-cooled wafer. Three fluorocarbon feedgas chemistries are compared, i.e., $CHF_3$ (40 sccm), $C_3F_6$ (40 sccm), and $C_3F_6/H_2$ (40 sccm/15 sccm) at 1400 W inductive power and 6 mTorr operating pressure. The processing time is proportional to the wafer temperature. For $C_3F_6$ the 600 W data are also included. The temperature/time correspondence is different in this case. (B) The etch rates of fluorocarbon films deposited at the same conditions at which they are etched are measured as a function of RF bias power at 1400 W inductive power, 6 mTorr operating pressure plasmas fed with various fluorocarbon gases, i.e., $CHF_3$ (40 sccm), $C_3F_6$ (40 sccm), and $C_3F_6$ $H_2$ (40 sccm/15 sccm).

### C. Temperature dependence of plasma–wall interactions

In order to study the temperature dependence of the processes occurring at a non-biased wall that has poor thermal contact, an experiment was performed on a non-biased wafer that is lifted above the chuck by three small Teflon studs. The thermal conductivity between the cooled electrostatic chuck and the wafer is poor in this case. The only energy loss factor is the Stefan-Boltzmann radiation from the wafer to the chuck. Apart from a dissimilarity due to differences in heat capacitance of the wafer and the confinement ring, the behavior of wafer and wall will be similar. The temperature of the wafer will increase with time until it reaches a maximum after which it will no longer change.

Figure 5(A) shows the results of this experiment performed in discharges fed with $CHF_3$ (40 sccm), $C_3F_6$ (40 sccm), and $C_3F_6/H_2$ (40 sccm/15 sccm) using 1400 W inductive power and 6 mTorr operating pressure. The fluorocarbon passive deposition rates are plotted as a function of processing time (i.e., increasing substrate temperature). The initial deposition rates are similar to the deposition rates obtained with a clamped wafer when a helium backside pressure is applied; see Fig. 5(B). As the processing continues, and thus

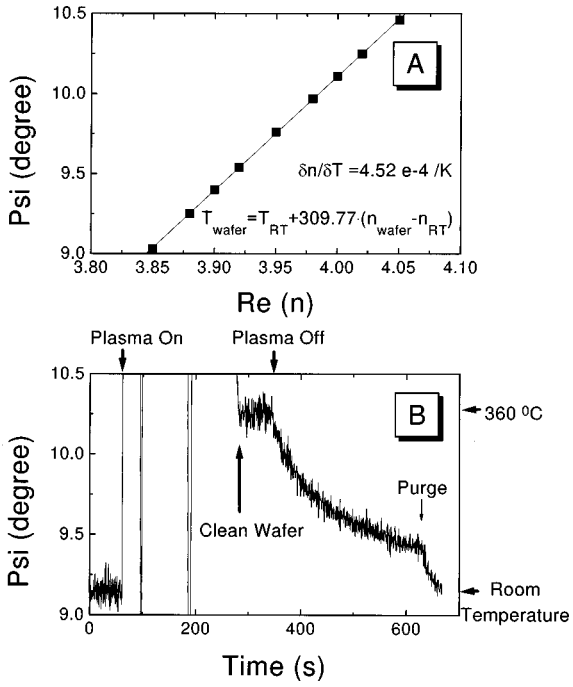


FIG. 6. (A) Simulated correlation between the ellipsometric angle $\Psi$ measured on a crystalline silicon wafer and the real part of the refractive index of the silicon. (B) Ellipsometric angle $\Psi$ measured as a function of time on a non-cooled crystalline silicon wafer in a $C_3F_6$ plasma at 1400 W inductive power and 6 mTorr operating pressure.

the temperature of the substrate increases, the deposition rate decreases until a point in time where no net deposition takes place. Beyond this point the deposited fluorocarbon material will be removed until no fluorocarbon is left on the *c*-Si wafer. It thus shows that on a surface with a temperature above a certain value no net deposition will take place.

The temperature rise of the non-cooled wafer is quantified by measuring the ellipsometric angle $\Psi$ on the hot, clean *c*-Si wafer after the $C_3F_6$ experiment from Fig. 5. The $\Psi$ angle is strongly related to the real part of the refractive index, Re($n$), of the silicon.[13] The correlation between $\Psi$ and Re($n$) is calculated using an ellipsometry simulation routine, and is plotted in Fig. 6(A). Using the temperature coefficient of Re($n$) of silicon at 632.8 nm, $\delta n/\delta T = 4.52 \times 10^{-4}\ \mathrm{K}^{-1}$, it can be calculated from the data in Fig. 6(B) that the temperature of the wafer, after all fluorocarbon material has been removed, is at a value around 360 °C. This temperature corresponds well with the stable wall temperature in a 1400 W, 6 mTorr plasma; see Fig. 4.

In Fig. 5 it is shown that the point where the net deposition rate is zero occurs earlier in time (i.e., at a lower temperature) for $C_3F_6$ (40 sccm) than for either $CHF_3$ (40 sccm), which has a much lower initial deposition rate, or $C_3F_6$ (40 sccm) with 15 sccm $H_2$ added to it, which has a similar initial deposition rate.

The results from this experiment allow an interesting analogy to be made between substrate temperature and RF bias power when etching fluorocarbon material deposited on a cooled wafer. The etch rate of fluorocarbon material (deposited at the same condition as etching is performed) as a function of RF bias power is plotted in Fig. 5(B). It shows that $C_3F_6$ has a lower threshold RF bias power for etching than $C_3F_6/H_2$ even though the passive deposition rates (i.e., 0 W RF bias power) are similar. It also shows that $CHF_3$ has a higher threshold RF bias power than $C_3F_6$, even though the passive deposition rate is significantly lower. From this comparison it can be suggested that, in fluorocarbon etching, the RF bias power and the substrate temperature play a similar role, i.e., an energy source for enabling chemical reactions. It further shows that the transition from deposition to etching is strongly dependent on the feedgas chemistry. The reason why $CHF_3$ and $C_3F_6/H_2$ deposited fluorocarbon films require a higher threshold RF bias power or a higher substrate temperature is due to differences in chemical composition. The F/C ratios of the $CHF_3$ and $C_3F_6/H_2$ fluorocarbon films are lower than the F/C ratio of $C_3F_6$ fluorocarbon material due to the fluorine scavenging effect of hydrogen.[12,14]

### D. Temperature dependence of the gas phase chemistry

The results from Sec. III C indicate that fluorocarbon species that are precursors for deposition on low temperature surfaces do not deposit on hot surfaces and remain in the plasma. The (low temperature surface) deposition precursor density thus increases. This is consistent with results from Chinzei *et al.*,[15] who reported that in a $C_4F_8$ ICP no polymer deposition occurs on surfaces at temperatures higher than 200 °C. The density of CF and $CF_2$ radicals, as measured by mass spectrometry, is one order of magnitude higher in a 200 °C heated reactor in comparison to a reactor at 30 °C. Hikosaka *et al.*[16] also reported mass spectrometric results showing that, as the temperature of their quartz wall increased, the $CF_3$ radical density increased due to a reduced surface loss of these species. They additionally found an increased CO density due to enhanced etching of the quartz wall at higher temperatures and a decrease in *F* density which they ascribed to the enhanced F absorption on the quartz wall. Fluorine absorption by an aluminum wall has also been reported by Chinzei *et al.* In mass spectrometry measurements Maruyama *et al.*[17] observed that for $CF_4$ plasmas an increase in the $CF_x$ radical density occurs as the wall temperature goes up. O'Neill and Singh[9] who performed ultraviolet (UV)-absorption spectroscopy in order to examine the $CF_2$ radical density in a $C_2F_6/CF_4$ plasma also reported a steady increase of this density as processing proceeds. They ascribed this effect to increasing polymer deposition on the wall, but also mentioned that the reactor wall temperature may play a significant role.

Figure 7 shows optical emission spectra taken on a 1400 W, 6 mTorr, 40 sccm $C_3F_6$ discharge in both a relatively cold (60 °C) and a hot (300 °C) reactor. Significant intensity differences can be observed in the emission from various carbon containing species. In Fig. 8 the peak intensities of $CF_2$, $C_2$, CO and also those of atomic fluorine and oxygen are plotted as a function of reactor wall temperature. The intensities are normalized to their value in a hot reactor.

It shows that the initial value, i.e., in a cold reactor, of the

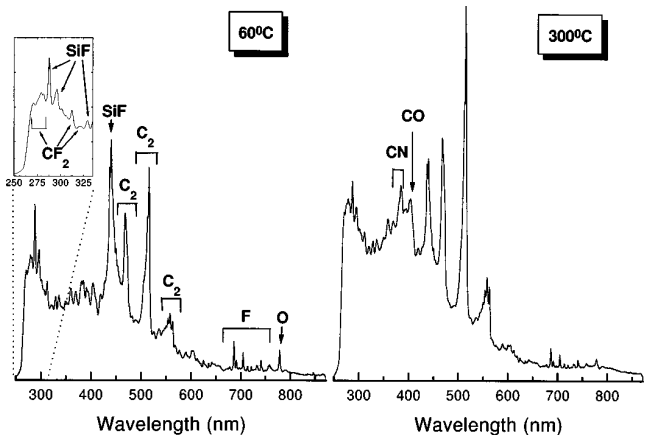


FIG. 7. Comparison of optical emission spectra measured on a $C_3F_6$ plasma at 1400 W inductive power and 6 mTorr operating pressure. The left panel shows the spectrum measured in a cold (60 °C) reactor and the right panel shows the spectrum measured in a hot (300 °C) reactor.

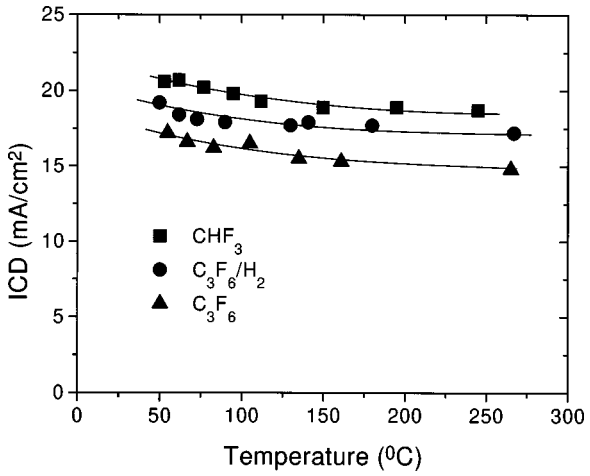


FIG. 9. Ion current density as a function of reactor wall temperature (1400 W inductive power, 6 mTorr operating pressure).

intensity of carbon containing species is around 50%–60% of the final, hot reactor value. The fluorine intensity is initially 10% higher than its final intensity. This indicates that the concentration ratio of carbon containing species, i.e., deposition precursors, over atomic fluorine, i.e., etch precursor, increases as the reactor temperature increases.

The increase in the CO intensity coincides with a decrease of the atomic oxygen signal. The CO formation can therefore be explained by an increased carbon density in the plasma reacting with atomic oxygen.

At a constant pressure, the particle density decreases as the reactor temperature increases. Therefore, the electron mean free path and thus the electron temperature will increase. The constant emission intensity at temperatures higher than 200 °C may therefore correspond to a decreasing radical density. A change in the electron temperature, however, should not influence the relative intensity of F emission to $CF_2$ and $C_2$, i.e., the gas phase F/C ratio, assuming approximately similar excitation cross sections for these species.

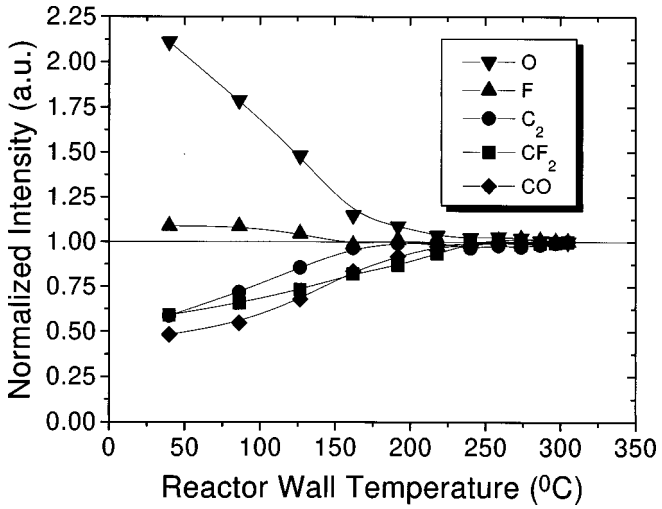


FIG. 8. Emission intensities measured in a $C_3F_6$ plasma at 1400 W inductive power and 6 mTorr operating pressure. The intensities of the various species are normalized to their value in a hot reactor.

### E. Temperature dependence of the ion current density

The ion current density has been measured as a function of reactor wall temperature in $CHF_3$, $C_3F_6$, and $C_3F_6/H_2$ discharges; see Fig. 9. The ion current density decreases as the wall temperature increases. The ion density may decrease more significantly as a function of reactor wall temperature than the ion current density does, assuming that the electron temperature increases. A higher electron temperature leads to an increase in the ion acoustic velocity, which results in a higher ion current density for a given ion density.

The decrease in the ion density can partially be explained by the fact that the overall particle density goes down as the temperature of the reactor walls increases.

### F. Temperature dependence of plasma-surface interactions

#### *1. Fluorocarbon deposition*

The results previously presented suggest a time dependence of the fluorocarbon deposition on cold surfaces, such as cooled substrates. Figure 10 shows the passive fluorocarbon deposition measured as a function of reactor wall temperature in a $C_3F_6$ (40 sccm) and $C_3F_6/H_2$ (40 sccm/12 sccm) plasma at 1400 W inductive power and 6 mTorr operating pressure. The deposition rate shows a maximum as a function of wall temperature. This can be explained as follows.

Initially passive deposition will take place on the walls at the same rate as on the wafer. As the walls heat up, the passive deposition rate on the walls will decrease and ultimately fluorocarbon removal will occur. The deposition precursor density in the gas phase increases at the same time, raising the passive deposition on the cooled wafer. After all the fluorocarbon material has been removed from the walls, the deposition precursor density in the gas phase and thus the

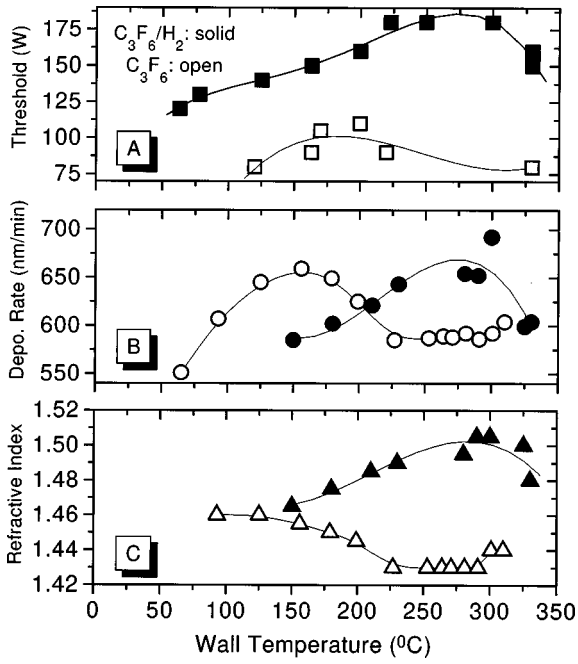


FIG. 10. (A) Threshold RF bias power for etching, (B) passive fluorocarbon deposition rate, and (C) the fluorocarbon refractive index as a function of reactor wall temperature in a $C_3F_6$ (40 sccm) and a $C_3F_6$ /$H_2$ (40 sccm/12 sccm) plasma at 1400 W inductive power and 6 mTorr operating pressure.

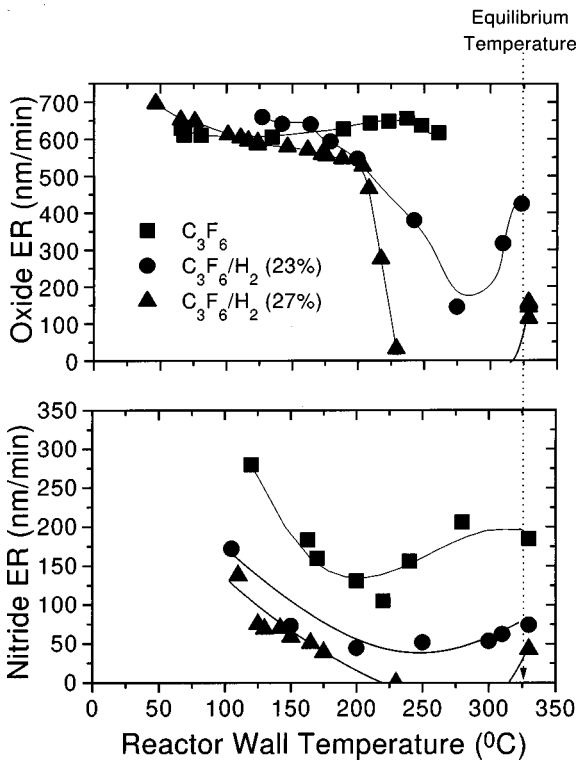


FIG. 11. (A) Oxide etch rates and (B) nitride etch rates as functions of wall temperature measured in $C_3F_6$ (40 sccm), $C_3F_6/H_2$ (40 sccm/12 sccm), and $C_3F_6/H_2$ (40 sccm/15 sccm) discharges at 1400 W inductive power and 6 mTorr operating pressure at a RF bias power of 200 W (i.e., −100 V self-bias).

passive deposition rate at the wafer will decrease again (but still be higher than the initial rate). This is consistent with results reported by Tsukada *et al.*,[18] who reported that polymer deposition on the coldest surface is faster than on other surfaces. The reason that the maximum in the deposition rate occurs at a higher temperature in $C_3F_6/H_2$ than in $C_3F_6$ is consistent with the data in Fig. 5, which show that a higher temperature is needed to remove fluorocarbon deposited in $C_3F_6/H_2$.

The refractive index of the deposited fluorocarbon material shown in Fig. 10 has been shown to be inversely proportional to the F/C ratio.[1] The maximum in deposition rate coincides with a maximum in the refractive index. Figure 10 also shows the temperature dependence of the threshold RF bias power, defined as the RF bias power at which net fluorocarbon deposition is prevented by ion bombardment, but no net substrate etching occurs. The data show that the etching of the fluorocarbon material is increasingly difficult as the fluorocarbon deposition rate increases and as the F/C ratio decreases. A maximum in the RF threshold bias power is observed at the same temperature as the maximum in the deposition rate and refractive index occurs.

### 2. Oxide etching

Figure 11(A) shows the oxide etch rates monitored for longer time periods than in Fig. 2 for $C_3F_6/H_2$ discharges at 1400 W inductive power, 6 mTorr operating pressure at −100 V self-bias voltage, and different $H_2$ additions. In the temperature regime up to 200 °C, the oxide etch rate is fairly temperature independent. It is also independent of the feedgas chemistry. The slight decrease in the etch rate can be explained by the decreasing ion current density since the oxide etch mechanism has been shown to be mainly ion driven.[6,19] For higher temperatures a strong dependence on feedgas chemistry is observed, which cannot be explained by direct reactive ion etching of the oxide. When 15 sccm of $H_2$ is added to 40 sccm of $C_3F_6$, the etch process goes into a deposition mode at a temperature of around 250 °C. For a $H_2$ addition of 12–40 sccm $C_3F_6$ the etch rate displays a minimum. For pure $C_3F_6$, the oxide etch rate is temperature independent.

The minimum in the etch rate at 12 sccm $H_2$ addition is consistent with the maximum in the passive deposition rate as a function of temperature. It is also consistent with the maximum in the fluorocarbon refractive index (minimum in F/C ratio). The minimum in the etch rate occurs also at 15 sccm $H_2$ addition, but then as a maximum in the deposition rate (under biased conditions).

The fact that for pure $C_3F_6$ no minimum in the oxide etch rate is seen, although there is a maximum in the passive deposition rate, indicates that the oxide etch mechanism is more complicated than just reactive ion sputtering.

An explanation for this behavior can be found by observing that the oxide etch rate as a function of self-bias voltage exhibits: (1) fluorocarbon deposition, (2) fluorocarbon suppression, and (3) oxide sputtering.[6,12,14] In the fluorocarbon deposition regime net fluorocarbon deposition takes place. As the RF bias power is increased and a larger self-bias

voltage develops, the fluorocarbon suppression regime is entered and oxide etching occurs. The sputtering mechanism is however suppressed by the presence of a relatively thick steady-state fluorocarbon film. As the RF bias power is further increased, the oxide surface becomes free of fluorocarbon material and chemical sputtering can occur. The etch rate is then proportional to the square root of the ion energy.

The dependence of the oxide etch rate on RF bias was examined for different fluorocarbon feedgas chemistries. The passive deposition rate is similar for both $C_3F_6$ and $C_3F_6/H_2$, but the RF bias threshold power for etching and the RF power at which the sputtering regime is reached are higher for $C_3F_6/H_2$. This is consistent with the etching of fluorocarbon material, as shown in Fig. 5. For sufficiently high RF bias powers the oxide etch rates in $C_3F_6$ and $C_3F_6/H_2$ are similar. At that point the sputtering regime is reached and the etching is mainly dependent on the ion flux to the surface. Figure 9 showed that the ion current densities for $C_3F_6$ and $C_3F_6/H_2$ are fairly similar.

In Fig. 10 the temperature dependence of the RF threshold power required to induce oxide etching in a $C_3F_6$ (40 sccm) and a $C_3F_6/H_2$ (40 sccm/12 sccm) discharge is shown. It shows a maximum, similar to the fluorocarbon deposition rate. This can be understood since at the etch threshold point the deposition and etching processes balance each other. If the deposition rate increases, one needs to compensate for this by increasing the bias. The opposite holds for a decrease in the threshold value.

### 3. Nitride and silicon etching

Figure 11(B) shows the nitride etch rate as a function of reactor wall temperature for $C_3F_6/H_2$ discharges at 1400 W inductive power, 6 mTorr operating pressure at −100 V self-bias voltage, and different $H_2$ additions. Figure 11(B) is consistent with Fig. 2. It shows that the nitride etch rate dependence on the reactor wall temperature is different from the oxide etch rate dependence. This can be explained by taking in account results obtained when nitride samples were etched as function of the RF bias power for $C_3F_6$ and $C_3F_6/H_2$. For RF bias powers where oxide was being etched by a sputtering mechanism, the nitride etching was suppressed, and the degree of suppression depended strongly on the feedgas chemistry. Similar results were obtained for silicon substrates with the difference that these were suppressed to an even lower level.[12,14,20]

### 4. Model

In Figure 12 all the above information is combined. It shows schematically the influence of increasing wall temperature on the oxide etch rate as a function of self-bias voltage in both the $C_3F_6$ and the $C_3F_6/H_2$ cases. As the passive deposition rate increases, the RF bias threshold shifts to a higher value. For the $C_3F_6$ case etching at 100 V self-bias (=200 W RF bias power) still occurs through the mechanism of oxide sputtering. No temperature dependence can therefore be observed; see Fig. 12(A). For $C_3F_6/H_2$, however,

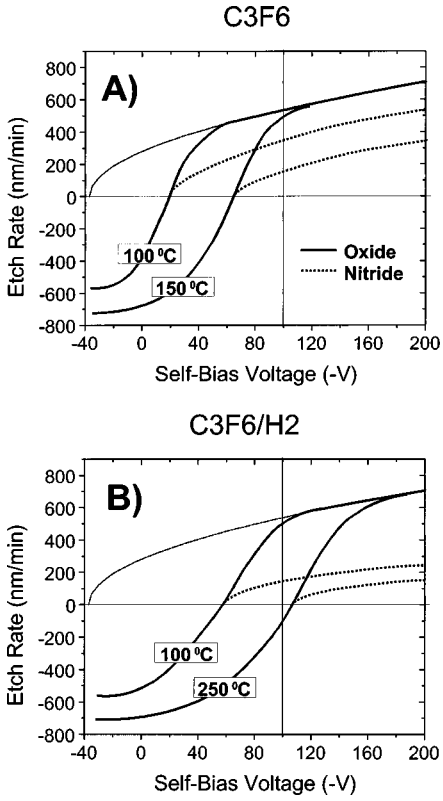


FIG. 12. Schematic view of the oxide and nitride etch characteristics for various wall temperatures for (A) $C_3F_6$ processing and (B) $C_3F_6$ /$H_2$ processing. The thick solid curves represent the oxide etching, and the dotted lines the nitride etching. The sputtering curve (thin solid line) is also included.

etching has shifted into the fluorocarbon suppression regime, resulting in a temperature dependent etch behavior; see Fig. 12(B).

Joubert *et al.*[21] used oxide etch rate versus self-bias voltage curves similar to the ones presented in Fig. 12 in order to explain reactive ion etching (RIE) lag effects. Since differential charging at the bottom of etched features occurs, ions entering the feature are retarded, resulting in a decreased etch yield or even deposition. It is expected that the reactor wall temperature effect will enhance the RIE lag effect significantly.

The wall temperature dependence of the nitride etch rate can also be explained using the information presented above. Figure 12 also schematically shows the effect of increasing wall temperature for both $C_3F_6$ and $C_3F_6/H_2$ on the nitride etch rate. As the passive deposition rate increases, the RF bias threshold shifts to a higher value, and the etch rate values at a certain self-bias voltage are being suppressed. This is the case for both $C_3F_6$, Fig. 12(A), and $C_3F_6/H_2$ etching, Fig. 12(B), at 100 V self-bias (=200 W RF bias power), resulting in a temperature dependent etch behavior. The same explanation holds for the silicon etching data.

It can thus be suggested that the increased reactor wall temperature results in a more efficient suppression of the substrate etch rate due to enhanced fluorocarbon deposition which leads to a thicker steady-state fluorocarbon film. The

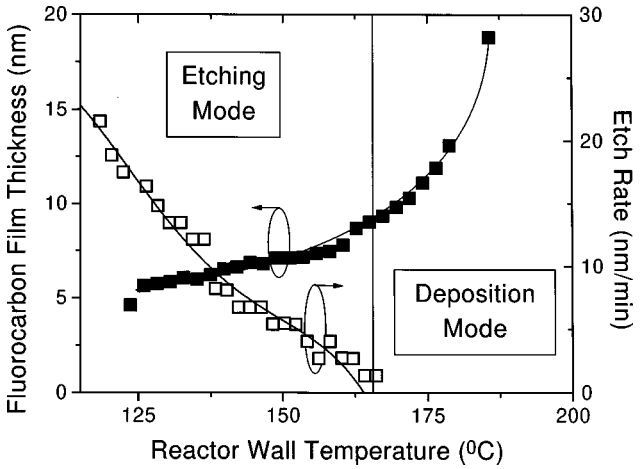


FIG. 13. The silicon etch rate and the thickness of the steady-state fluorocarbon film measured as a function of reactor wall temperature. As the film thickness increases, the silicon etch rate decreases (1400 W, 6 mTorr, −100 V self-bias).

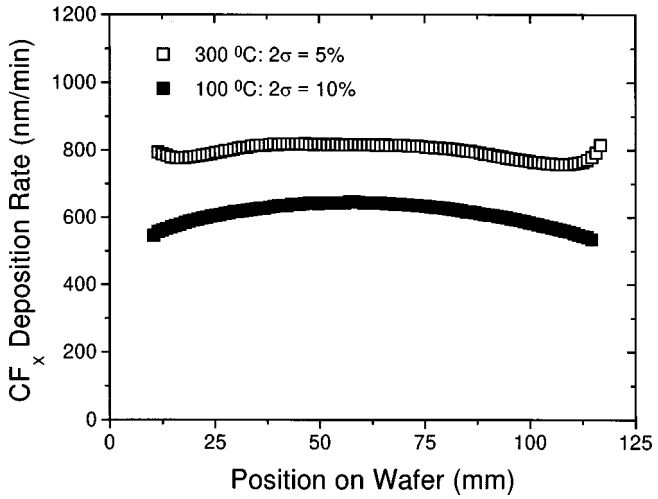


FIG. 14. The fluorocarbon deposition rate profiles as a function of position on the wafer obtained in a $C_3F_6/H_2$ (40 sccm/15 sccm) discharge at 1400 W inductive power and 6 mTorr operating pressure. The open symbols correspond to a condition where the reactor wall temperature is around 300 °C. For the solid symbols the reactor wall temperature is around 100 °C. The fluorocarbon deposition uniformity is 10% ($2\sigma$) at 100 °C and 5% ($2\sigma$) at 300 °C.

suggested mechanism is supported by the data in Fig. 13, which show the silicon etch rate and the steady-state fluorocarbon film thickness (determined by ellipsometry) as a function of reactor wall temperature in a $C_3F_6/H_2$ plasma at 1400 W inductive power and 6 mTorr operating pressure. The silicon etch rate decreases as the fluorocarbon film thickness increases until the process moves from an etching mode into a deposition mode. This is consistent with results from other studies that report that the etch rate of a substrate is inversely proportional to the fluorocarbon film thickness.[12,14,20]

### G. Temperature dependence of process uniformity

In the above it has been shown that the fluorocarbon deposition rate is a key parameter in the selective oxide etching process. The temperature dependence of the process uniformity is now investigated by measuring the fluorocarbon deposition rate as a function of position on the wafer (using *ex situ* spatially resolved ellipsometry). In Fig. 14 the fluorocarbon deposition rate profile obtained in a $C_3F_6/H_2$ (40 sccm/15 sccm) discharge at 1400 W inductive power and 6 mTorr operating pressure in a reactor with a wall temperature of 100 °C is compared to the profile obtained at 300 °C. The fluorocarbon deposition rate in the 300 ° C case is found to be higher than that in the 100 ° C case at all positions on the wafer.

The deposition rate at 100 °C is maximum in the center and decreases when moving away from the center. The fluorocarbon deposition uniformity is 10% ($2\sigma$) over the analyzed diameter of 115 mm. The difference in deposition rate between the 300 and 100 °C cases is found to be lowest in the center of the wafer and increases when moving away from the center. This can be explained by the fact that in a cold reactor the reactor wall acts as a sink for deposition precursors, while at higher temperatures the deposition precursors are recycled into the discharge. At this operating pressure it is more likely that species leave the sidewall and reach the wafer without undergoing a gas-phase collision at positions further from the center.[8] As a result of this, the fluorocarbon deposition profile at 300 °C is more uniform, i.e., 5% ($2\sigma$) over the scanned diameter of 115 mm.

## IV. CONCLUSIONS

The influence of reactor wall conditions on the stability of etch processes in an inductively coupled fluorocarbon plasma has been studied. The results indicate that reactor wall temperature is an important parameter in these etch processes. A model that describes the time dependence of the reactor wall temperature has been developed and fitted to experimental data.

The fluorocarbon deposition rate onto the wall is strongly dependent on the wall temperature. If the wall has a temperature higher than a certain feedgas chemistry dependent value, no net deposition will occur. The deposition on cold surfaces, e.g., the cooled wafer, increases as the fluorocarbon deposition on the walls decreases due to an increase in the gas-phase deposition precursor density. This requires an increase in the RF bias power to maintain a stable oxide etch rate in highly polymerizing gas mixtures, such as $C_3F_6/H_2$. A strong suppression of the nitride and silicon etch rates is seen and can be explained by the same mechanism.

This work shows that adequate control of the reactor wall temperature is required to maintain process stability and to improve oxide to nitride/silicon etch selectivity and process uniformity.

## ACKNOWLEDGMENTS

This work was financially supported by Lam Research Corporation and the New York State Science and Technology Foundation. The authors would like to acknowledge R. J. Severens, M. C. M. v.d. Sanden, and D. C. Schram from

the Eindhoven University of Technology for helpful discussions. N. R. Rueger, M. F. Doemling, and J. M. Mirza are thanked for sharing insights obtained in their parallel studies performed in the ICP in the Plasma Processing and Research Laboratories at the University at Albany. The authors also would like to thank the NUFFIC for their STIR-WO grant and Eindhoven University of Technology for their Mignot grant, which allows for the exchange of students between Eindhoven University of Technology and the State University of New York at Albany.

[1]J. M. Cook, IEEE/SEMI 1995 Advanced Semiconductor Manufacturing Conference and Workshop, Theme—Semiconductor Manufacturing: Economic Solutions for the 21st Century, AMSC '95 Proceedings (Cat. No. 95CH35811) (1) 1995, p. 391.
[2]G. S. Oehrlein, Y. Zhang, D. Vender, and M. Haverlag, J. Vac. Sci. Technol. A **11**, 323 (1993).
[3]G. S. Oehrlein, Y. Zhang, D. Vender, and O. Joubert, J. Vac. Sci. Technol. A **11**, 333 (1993).
[4]F. H. Bell, O. Joubert, G. S. Oehrlein, Y. Zhang, and D. Vender, J. Vac. Sci. Technol. A **12**, 3095 (1994).
[5]Y. Zhang, G. S. Oehrlein, and F. H. Bell, J. Vac. Sci. Technol. A **14**, 2127 (1996).
[6]N. R. Rueger, J. J. Beulens, M. Schaepkens, M. F. Doemling, J. Mirza, T. E. F. M. Standaert, and G. S. Oehrlein, J. Vac. Sci. Technol. A **15**, 1881 (1997).
[7]M. F. Doemling, N. R. Rueger, J. M. Cook, and G. S. Oehrlein, J. Vac. Sci. Technol. (submitted).
[8]S. C. McNevin, K. V. Guinn, and J. Ashley Taylor, J. Vac. Sci. Technol. B **15**, 214 (1997).
[9]J. A. O'Neill and J. Singh, J. Appl. Phys. **77**, 497 (1995).
[10]J. H. Keller, J. C. Foster, and M. S. Barnes, J. Vac. Sci. Technol. A **11**, 2487 (1993).
[11]J. A. Meyer, K. H. R. Kirmse, J.-S. Jenq, S. Y. Perez-Montero, H. L. Maynard, A. E. Wendt, J. W. Taylor, and N. Hershkowitz, Appl. Phys. Lett. **64**, 1926 (1994).
[12]M. Schaepkens, T. E. F. M. Standaert, P. G. M. Sebel, J. M. Cook, and G. S. Oehrlein (unpublished).
[13]G. M. W. Kroesen, G. S. Oehrlein, and T. D. Bestwick, J. Appl. Phys. **69**, 3390 (1991).
[14]M. Schaepkens, Masters thesis, Eindhoven University of Technology VDF/NT 96-23, 1996, p. 47.
[15]Y. Chinzei, T. Ichiki, R. Kurosaki, J. Kikuchi, N. Ikegami, T. Fukazawa, H. Shindo, and Y. Horiike, Jpn. J. Appl. Phys., Part 1 **35**, 2472 (1996).
[16]Y. Hikosaka, M. Nakamura, and H. Sugai, Jpn. J. Appl. Phys., Part 1 **33**, 2157 (1994).
[17]T. Maruyama, N. Fujiwara, K. Siozawa, and M. Yoneda, Jpn. J. Appl. Phys., Part 1 **35**, 2463 (1996).
[18]T. Tsukada, S. Mashiro, and K. Mashimo, Jpn. J. Appl. Phys., Part 1 **32**, 4850 (1993).
[19]G. S. Oehrlein, P. J. Matsuo, M. F. Doemling, N. R. Rueger, B. E. E. Kastenmeier, M. Schaepkens, Th. Standaert, and J. J. Beulens, Plasma Sources Sci. Technol. **5**, 193 (1996).
[20]T. E. F. M. Standaert, M. Schaepkens, P. G. M. Sebel, J. M. Cook, and G. S. Oehrlein, J. Vac. Sci. Technol. A **16**, 239 (1998).
[21]O. Joubert, G. S. Oehrlein, and M. Surendra, J. Vac. Sci. Technol. A **12**, 665 (1994).